https://doi.org/10.5194/acp-2020-1284
Preprint. Discussion started: 18 January 2021

Atmospheric Chemistry and Physics Discussions

Aerosol Effects on Electrification and Lightning Discharges in a Multicell Thunderstorm Simulated by the WRF-ELEC Model

Mengyu Sun[1,5], Dongxia Liu[1], Xiushu Qie[1], Edward R. Mansell[2], Yoav Yair[3], Alexandre O. Fierro[2,4], Shanfeng Yuan[1], Zhixiong Chen[1,5], Dongfang Wang[1]

[1] Key Laboratory of Middle Atmosphere and Global Environment Observation, Institute of Atmospheric Physics, Chinese Academy of Sciences, Beijing, China

[2] NOAA/National Severe Storms Laboratory, Norman, Oklahoma, USA

[3] Interdisciplinary Center (IDC) Herzliya, School of Sustainability, Herzliya, Israel

[4] Cooperative Institute for Mesoscale Meteorological Studies, University of Oklahoma, Norman, Oklahoma, USA

[5] College of Earth and Planetary Sciences, University of Chinese Academy of Sciences, Beijing, China

Correspondence to: Dongxia Liu (liudx@mail.iap.ac.cn)

Abstract

To investigate the effects of aerosol on lightning activity, the Weather Research and Forecasting (WRF) Model with a two-moment bulk microphysical scheme and bulk lightning model was employed to simulate a multicell thunderstorm that occurred in the metropolitan Beijing area. The results suggest that under polluted condition lightning activity is significantly enhanced during the developing and mature stages, while it is being delayed at the initial stage. Electrification and lightning discharges within the thunderstorm show distinguish characteristics by different aerosol conditions through microphysical processes. Elevated aerosol loading increases the cloud droplets numbers, the latent heat release, updraft and ice-phase particle number concentrations. More

https://doi.org/10.5194/acp-2020-1284
Preprint. Discussion started: 18 January 2021

Atmospheric Chemistry and Physics Discussions

negative charges in the upper level are carried by ice particles and enhance the electrification process. A larger effective radius of graupel particles further increases non-inductive charging due to more effective collisions. The first lightning discharge was delayed at the beginning of polluted thunderstorm, coincident with the delayed occurrence of graupel and ice particles, which are responsible for charge generation through the non-inductive mechanism. In the continental case where aerosol concentrations are low, less latent heat releases in the upper parts of the cloud and as a consequence, the updraft speed is weaker leading to smaller concentrations of ice particles, lower charging rates and less lightning discharges.

1 Introduction

Lightning activity is related to two important factors: dynamic-thermodynamic and microphysical characteristics (e.g. Williams et al., 2005; Guo et al., 2016; Wang et al., 2018; Zhao et al., 2020). Since the dynamic-thermodynamic processes affect the development of thunderstorm significantly, lightning activity is influenced by various dynamic-thermodynamic variables: temperature (Price, 1993), relative humidity in the lower and middle troposphere (Xiong et al., 2006; Fan et al., 2007), and convective available potential energy (Qie et al., 2004; Stolz et al., 2015), and many others.

The impacts of aerosol on the development of thunderstorm especially in metropolitan areas have been researched extensively. Observational studies indicated that the enhancement of lightning activity was related to increased cloud condensation nuclei (CCN) concentration (e.g., Westcott, 1995; Orville et al., 2001; Kar et al., 2009; Wang et al., 2011; Chaudhuri and Middey, 2013; Thornton et al., 2017; Yair, 2018). Kar et al. (2009) found a positive correlation between PM10 and SO_2 concentration and lightning flash densities around major cities in South Korea. A positive relationship between levels of particle pollution and lightning flash counts was also indicated by Chaudhuri and Middey (2013).

Furthermore, a variety of numerical simulations (e.g., Mitzeva et al., 2006) demonstrated the effects of aerosol on enhancing lightning activity. Using the Weather

https://doi.org/10.5194/acp-2020-1284
Preprint. Discussion started: 18 January 2021

Research and Forecasting (WRF) Model with explicit spectral bin microphysics, Khain et al. (2010) found elevated aerosol increased the number of cloud droplets and the release of latent heat by acting as CCN. Therefore, more liquid water was lifted to mixed-phase region by strong updrafts, with more ice-phase particles produced which can affect charge separation and lightning formation (Takahashi, 1978; Saunders and Peck, 1998; Takahashi et al., 1983; Mansell et al., 2005; Yair, 2008). Mansell and Ziegler (2013) suggested that greater CCN concentration led to greater lightning activity up to a point by testing a wide range of CCN concentration in a 3D model with two-moment bulk microphysics and stochastic branched discharge parameterization (Mansell et al., 2002). They also noted that average graupel density stayed high at lower CCN, but dropped at higher CCN because smaller droplets caused lower rime density. Zhao et al. (2015) showed that enhancing aerosol concentration resulted in an enhancement of electrification processes, due to the increasing growth rate of snow and graupel particles. However, Tan et al. (2017) simulated a thunderstorm in Changchun city with a 3D cumulus model coupled with aerosol module, electrification and lightning discharge, showing that the ice crystal and graupel number increased while the graupel mixing ratio decreased as the aerosol concentration increased.

The microphysical processes under different CCN concentration, especially the initiation and growth of ice-phase particles varied from different simulation studies. There are few studies that discussed the aerosol effects on thunderstorm with explicit electrification and discharge parameterization in the model simultaneously (e.g., Mitzeva et al., 2006; Mansell and Ziegler, 2013; Zhao et al., 2015). Simulation by Tan et al. (2017) showed that elevated aerosol loading delayed the first discharge but rarely analyzing the microphysical reasons. The detailed effects of aerosol on the delay of discharging need further study.

By analyzing lightning data from the Beijing Lightning Network (BLNET) and PM2.5 data, Sun et al. (2020) found a positive relationship between flash counts and PM2.5 concentration prior to the occurrence of thunderstorm. As a mega city, Beijing has higher aerosol concentration resulting from anthropogenic air pollution. Still, the effects of aerosol on both electrification and discharges have been rarely discussed in

https://doi.org/10.5194/acp-2020-1284
Preprint. Discussion started: 18 January 2021

Atmospheric Chemistry and Physics Discussions

this area by numerical simulation. Therefore, in this paper we present sensitivity studies on how the different CCN concentration influence the characteristic of thundercloud over the metropolitan Beijing area using the WRF-ELEC (Fierro et al., 2013). We conducted sensitivity studies to evaluate the response of the microphysical properties, as well as electrification and lightning processes to aerosol characteristics. This paper is organized as follows: section 2 describes the data and methodology used in the study, section 3 introduces the design of simulations, section 4 presents the results, and section 5 discusses and summarizes the study.

2 Data sources

2.1 Lightning data

Total flash numbers were obtained from the Beijing Lightning Network (BLNET), which consists of 16 stations covering East-West 110 km and North-South 120 km areas since 2015. The BLNET provides 3D-location results of flashes, including both intra-cloud (IC) and cloud-to-ground (CG) lightning (Wang et al., 2016). The average detection efficiency of the BLNET is 93.2% for the total flashes (Srivastava et al., 2017). In this study, the 3D-location lightning radiation pulses were grouped in flashes based on the criteria of 400 ms and 15 km. This grouping criteria was modified from the algorithm in Srivastava et al. (2017). In section 3, the lightning frequency from BLNET was calculated in every 6 min intervals, corresponding to the time span of Doppler radar scanning.

2.2 Radar data

In addition, the radar reflectivity data was obtained from an S-band Doppler radar (Chinese CINRAD/SA) near Beijing urban area (39.81 °N, 116.47 °E), and were updated every 6 min. The vertical levels vary from 500 m to 20 km and were processed into composite radar reflectivity with a horizontal resolution (0.01 °×0.01 °).

https://doi.org/10.5194/acp-2020-1284
Preprint. Discussion started: 18 January 2021

Atmospheric Chemistry and Physics
Discussions
Open Access

2.3 Synoptic background

A mesoscale convective system over the Beijing area influenced by a strong Mongolia cold vortex on 11 Aug 2017 was simulated in this study. Based on the weather map at 00:00 UTC (figure not shown), there was a prevailing westward airflow in the south of the cold vortex, which brought dry cold air in middle layer. At low-level of 850 hPa, the southwesterly jet transported warm and humid air mass, forming an unstable condition together with cold air mass above. The sounding profile over Beijing (39.9 °N, 116.2 °E) exhibited an unstable thermodyn[illegible] [illegible]r thunderstorm initialization, as shown in Fig. 1, with a surface [illegible] [illegible]ble potential energy (CAPE) of 3937 J kg^{-1} at 12:00 UTC. [illegible] [illegible]ndition with mountain in the northwest and ocean in the south[illegible] [illegible]), as well as heat island effect and elevated aerosol loading in the ur[illegible] [illegible] enhanced the convection and were responsible for the occurre[illegible] [illegible]d intensive lightning activity in the Beijing area. According to [illegible] [illegible]atic weather observation network in Beijing, the average rainf[illegible] [illegible] and the eastern region was 10-30 mm, with locally exceeding 100 mm. The maximum total lightning frequency even exceeded 1600 flashes (6 min)$^{-1}$ at the mature stage.

3. Model overview

The WRF (version 3.9.1) model coupled with bulk ligh[illegible] et al., 2013) and a two-moment bulk microphysics sche[illegible] Mansell and Ziegler, 2013) was used to simulate the m[illegible] occurred on 11 August 2017 in the Beijing metropolitan area.

The two-moment bulk microphysics scheme predicts bot[illegible] number concentration for a range of hydrometeor species ([illegible] snow, graupel, and hail). The graupel growth process conta[illegible]e following processes: collection of ice crystals by graupel, collection of snow particles by graupel, deposition of vapor to graupel, collection of supercooled water (cloud droplets and/or raindrops)

https://doi.org/10.5194/acp-2020-1284
Preprint. Discussion started: 18 January 2021

Atmospheric Chemistry and Physics
Discussions

by graupel, and conversions between hydrometeors. The CCN concentration is predicted as a bulk activation spectrum and initially mixed well vertically. The initiation of cloud droplets (both for cloud base and in-cloud) uses an expression based on Twomey (1959).

Explicit charging physics includes both non-inductive charging (Saunders and Peck, 1998) and inductive or polarization charging (Ziegler et al., 1991). Non-inductive charge separation resulting from rebounding collisions between graupel-hail and snow-cloud ice are all parameterized (Mansell et al., 2005). Numerical experiments (Mansell et al., 2010) found that total inductive charging is about an order of magnitude weaker than non-inductive charging, but can be important for lower charge regions. Only collisions between cloud droplets and ice-phase particles (graupel, ice, hail) are considered for inductive electrification. The discharge model parameterization from Ziegler and MacGorman (1994) is used within a cylindrical region (Fierro et al. 2013), whereby a flash would be initiated when the electric field exceeds a breakdown threshold at a model grid point (from here on, we shall use the term 'grids' for short). An estimate of flash origin density (*FOD*) rate (over a time period $T = t_2 - t_1$) is computed following Eq. (1) of Fierro et al. (2013):

$$FOD(T) = \frac{G}{C}\int_{t_1}^{t_2} B(t)dt, \quad (1)$$

where G is the horizontal grid cell area, C the cylinder cross sectional area and the integral represents the sum of all discharge locations $[B(t)]$ counts for all the time steps within the time period *T*. Further, lightning discharge events (*LDE*) are given by Eq. (2) of Fierro et al. (2013). Thus, the predicted lightning frequency over the Beijing area in section 3 is the *LDE* calculated in 6 min intervals:

$$LDE(T) = \sum FOD(T). \quad (2)$$

https://doi.org/10.5194/acp-2020-1284
Preprint. Discussion started: 18 January 2021

Atmospheric Chemistry and Physics
Open Access
Discussions

3.1 Design of the simulations

The nested model configuration for the simulations are shown in Table 1. The 1°×1° NCEP GFS (Global Forecast System) data is used to estab itial and boundary conditions.

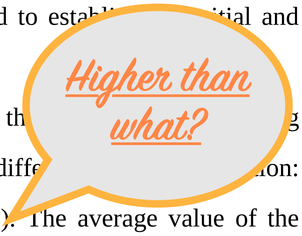

To survey the aerosol effects on the structure of th g activity, two sensitivity experiments are performed with diffe ion: a polluted case (P-case) and a continental case (C-case). The average value of the observed aerosol concentration before the thunderstorm initiation is much higher in the Beijing area (Sun et al., 2020), therefore, the CCN concentration is selected as the P-case which is consistent with observation. The initial value for the P-case is set as a number mixing ratio relative to sea level air density ρ_0: $2000/\rho_0$ kg^{-1}, where ρ_0=1.225, and the local number concentration is $2000\times(\rho_{air}/\rho_0)$ cm^{-3}. An er concentration for the C-case is set at $1200\times(\rho_{air}/\rho_0)$ cm^{-3}, co conditions (e.g. Hobbs and Rangno, 1985; Mansell et al., 2 communication, 2019). The relatively high prescribed CCN c eed small droplet diameters and effectively delayed the warm rain process in the model (Mansell and Ziegler, 2013).

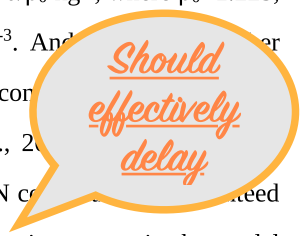

4 Results

4.1 Radar reflectivity and lightning flashes of multic

Figure 2 shows the observed and simulated radar r periods for both cases, with the formation of thunderstorms i the simulation earlier than the observation about 1.5 h. For this reason, we display the simulation and observation with ~90 minutes time difference. It is clear that both simulated times exhibit an overall good agreement with the evolution and morphology of the radar echo, especially evidenced by the northeast-southwest orientation of the radar echo at 11:54 UTC in the simulated (13:24 UTC in the observation) reflectivity fields. Note that the modeled reflectivity

https://doi.org/10.5194/acp-2020-1284
Preprint. Discussion started: 18 January 2021

differs from the observation in the northwestern area (116.4 °E-116.0 °E, Fig. 2a, 2c and 2e), and so the impacts of aerosol on lightning activity will only be evaluated in the southeastern Beijing area (116.0 °E-117.5 °E).

The temporal variation of total flashes from BLNET is shown in Figure 3a, including both intra-cloud (IC) and cloud-to-ground (CG) lightning. The lightning frequency gradually increased during 11:00-12:00 UTC and raised significantly after 12:00 UTC, as well as reached the peak value at 12:30 UTC, and then decreased gradually. According to the evolution of radar reflectivity and lightning activity, the thunderstorm was divided into four periods: the beginning 11:00 UTC), the developing stage (11:00-12:30 UTC), the mature) and the dissipating stage (after 13:30 UTC) of the thunders ution of predicted lightning frequency over Beijing area under t ental cases are shown in Fig. 3b, both of them start earlier than observation about 1.5 h. The variation of flashes in the P-case is better consistent with the observation. In contrast, the occurrence of the first lightning for the continental case is earlier than both the observation and the polluted case.

Figure 4 displays the number of ini r the C-case and P-case during different periods. To e to aerosol, the intensity of lightning activity he lightning grids in each time step: light (50-100 avy (200-300 grids) and extreme (>300 grids). T d columns) in each category is counted hourly as the 'number of initiations'. A comparison of the different intensity categories reveals that the simulated lightning activities increase during 10:30-11:30 UTC (Fig. 4c) under high aerosol loading, corresponding to the developing and mature stages of the thunderstorm. During 09:30-10:30 UTC, while different categories of lightning are enhanced for both P- and C-case (Fig. 4b), it is noted that the maximum lightning initiation occurs in the extreme level for the P-case. There is no lightning initiation for the P-case at the beginning of the thunderstorm (08:30-09:30 UTC, Fig. 4a), however, all categories of lightning are initiated in the C-case, indicating that the first discharging is delayed under polluted condition. This phenomenon is accordant

https://doi.org/10.5194/acp-2020-1284
Preprint. Discussion started: 18 January 2021

with previous simulation by Tan et al. (2017), which suggested that the first discharge time of the polluted thundercloud was delayed.

Hence, the results indicate that while elevated aerosol loading enhances lightning activities in the developing and mature stages of thunderstorm, the time of the first discharge is delayed. In the following contents we will offer a possible explanation for this effect.

4.2 Microphysical properties of multicell

To investigate the effects of aerosol on lightning activities, we first analyze the simulated microphysical properties in both the continental and polluted sensitivity studies. Figure 5a-5h show the temporal variations of mass mixing ratio and number concentration for different categories of hydrometeors with the vertical profiles, herein, their mass mixing ratios are averaged horizontally. Figure 5i-5j show the time-height plots of maximum radar reflectivity and vertical velocities. The time-height plots of cloud droplets (Fig. 5a, 5b), raindrops (Fig. 5c, 5d), graupel (Fig. 5e, 5f) and maximum radar reflectivity (Fig. 5i, 5j) in both c a occur at about 09:00 UTC, 10:00 UTC, and 11:30 nt stages of the thunderstorm.

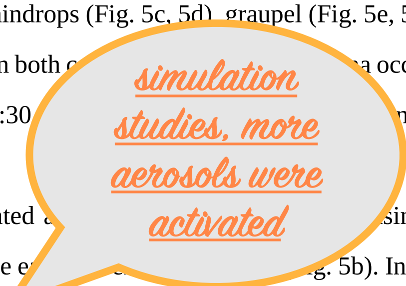

It can be seen that elevated a sing cloud droplets concentrations especially at the e g. 5b). In previous studies, more aerosols could be activated into cloud d water vapor condenses onto these droplets, leading to large clou l droplet size under polluted condition (Lynn et al., 2007; Wa ., 2015; Jiang et al., 2017). However, in this study, more clou case probably not result from condensation but come from less conversion to raindrops. This is because the CCN concentration in the C-case is already high and the supersaturations are probably close to zero after condensation of water vapor. The additional CCN in the P-case could not lead to further condensation, which is also evidenced by the similar vertical profiles of latent heating in both cases at 2-10 km, as shown in Fig. 10. Therefore, the more cloud

https://doi.org/10.5194/acp-2020-1284
Preprint. Discussion started: 18 January 2021

Atmospheric Chemistry and Physics Discussions
Open Access
EGU

droplets could not simply be explained by more condensation. The domain-averaged effective radius for cloud droplets is displayed in Fig. 6a, with small [illegible] dii under polluted condition. The maximum effective radii of cloud [illegible] 8.98 μm and 9.50 μm in different [illegible] and 7.42 μm for the poll [illegible] suppresses collection/co [illegible] ops in turn keeps more mass in drop [illegible] oud water in the P-case at early stages.

Consequently, th [illegible] warm rain process is delayed and the rainwater mass mixing ratio is less in the polluted case compared with the continent [illegible] droplets, which are to [illegible] rted into raindrops [illegible] freezing level. Pre [illegible] simulations fou [illegible] crystals could be [illegible] ndition, resulti [illegible] ation latent heat and stre [illegible] ain et al., 2008; Koren et al., 2010). In this study, the cloud d [illegible] on and corresponding latent heat in both cases are approximately the same. More mass loading of droplets in the P-case, however, might lead to weak updrafts at lower level (Fig. 5j). The cloud ice content is still higher in the P-case, probably owing to higher droplets content and [illegible] ing. As shown in Fig. 5h, the mass mixing ratio of ice crystals gr [illegible] lopment of thunderstorm, with domain-average of 12. [illegible] se and 11.39×10^{-2} g kg^{-1} for the continental case at the [illegible] UTC).

In contrast, the mass mixing ratio of graupel was relatively less in the P-case (Fig. 5f). Less graupel content under polluted condition is rather surprising, since previous simulation studies (Wang et al., 2011; Zhao et al., 2015) found th [illegible] e more graupel at the mature stage of thunderstorm, by virtue of enha [illegible] re cloud droplets lifted to the mixed-phase region. These coul [illegible] a much lower CCN concentration (< 400 cm^{-3}), in this [illegible] CCN concentration (> 1000 cm^{-3}), the reduced raindrops freezing (Fig. 5d) probably explain the lower density of graupel. Lower fall speed of the lower density graupel further results in less riming. Other simulation also found a decrease of graupel mixing ratio

https://doi.org/10.5194/acp-2020-1284
Preprint. Discussion started: 18 January 2021

under polluted condition, and partly [illegible] melting of graupel particles (Tan et al., 2017). Howe[illegible] of graupel in the polluted case is much larger compar[illegible]cially at the mature stage. The mean mixing ratio at the [illegible]ges were 17.23×10^{-3} g kg^{-1}, 41.70×10^{-3} g kg^{-1} for the P-case, and 8.31×10^{-3} g kg^{-1} and 41.53×10^{-3} g kg^{-1} for the C-case, respectively. Such a phenomenon partly explains the appearance of graupel of larger effective radius in the P-case (Fig. 6c). The effective radii of graupel reached 0.98 mm and 0.92 mm for the P-case, corresponding to 0.71 mm and 0.61 mm in different stages for the C-case. Compared to the small difference in effective radii of ice crystals between the polluted and continental cases (Fig. 6d), the radius of graupel is much larger in the P-case, which likely resulted in [illegible]arger collision efficiency between graupel particles and other ic[illegible]on-inductive charging.

No real differences at the dissipating stage

Increasing aerosol loading affect[illegible]rocesses, especially the ice-phase processes with n[illegible]l size. Both of them would inevitably affect lightn[illegible] rate and magnitude of electrification.

This is a conclusion, rather than a result

4.3 The relationship between hydrometeors and electrification

To analyze the relationship between hydrometeors and electrification, vertical cross sections is shown in Figure 7a and 8a, which display the total charge distribution at the mature stage of the thunderstorm in the polluted (11:54 UTC) and continental (11:24 UTC) cases. In the polluted case, a negative charge re[illegible]pper level (> 13 km), with the positive and negative charge cente[illegible]d lower level, respectively. The dipolar charge structure with p[illegible]er level and negative charge in the lower level simulated in the [illegible]assified as simple dipoles or tripoles (Williams et al., 1989) and, is more consistent with previous observations (Thomas et al., 2001) and simulations (Fierro et al., 2013; Zhao et al., 2015). As for the total net space charge density, the maximum of positive charge

How is it more consistent?

https://doi.org/10.5194/acp-2020-1284
Preprint. Discussion started: 18 January 2021

Atmospheric Chemistry and Physics Discussions

density at the mature stage in the P-case is up to +1 nC m^{-3}, which [illegible] than that in the C-case (< +0.5 nC m^{-3}).

We attempt to explain the origins of the charge distr[illegible] polarity and amount of charge carried by different hydromete[illegible] ice, graupel, snow and hail particles). The negative charge region in the upper level (12-15 km) results from collision of graupel with smaller ice crystals and snow particles (Fig. 7d), with the 30 dBZ echo tops reaching 13 km. The simulated vertical distribution of net charge in the C-case is caused by ice and snow particles charged positively at 8-13 km and graupel particles charged negatively at 4-10 km, respectively (Fig. 8b and 8d). However, less ice-phase particles appear in upper level in the C-case, corresponding to a relatively weaker negative charge center. Figure 7c and 8c show the cross sections of the simulated radar reflectivity and vertical velocity at 11:54 UTC (11:24 UTC) under different aerosol conditions. It is evident that both updraft and downdr[illegible] the polluted case at higher level are greater than that in the continental [illegible]ore freezing of droplets to ice-phase particles, and as a conseque[illegible]ty is significantly larger above 12 km.

Figure 7d shows that graupel and hail particles charg[illegible] negatively at 4-8 km, as a result of the non-inductive charging within region of relatively weak updrafts (< 5 m s^{-1}) in the P-case (Saunders and Peck, 1998). With large liquid water content (LWC) in the polluted case, graupel, ice and hail were charged positively, forming an intense positive charge center at 9km (< -20 ℃), as shown in Fig. 7a. The simulations show that non-inductive charging mechanism plays a main role at the mature stage, the rate of which is one order of magnitude larger than inductive charging (Fig. 9). As described in section 4.2, more ice particles and graupel with larger radii appear at this stage in the P-case, evidenced by the larger simulated radar reflectivity (Fig.7c), and the ensuing collision rates led to significantly stronger non-inductive charging at 6-10 km (Fig. 9b). In consequence, it is obvious from Fig. 7a and 8a that the charge density for the P-case is much higher than the C-case, indicating that aerosol plays an important role in affecting the accumulated charge density through microphysical and electrical processes.

https://doi.org/10.5194/acp-2020-1284
Preprint. Discussion started: 18 January 2021

The appearance of more ice-phase particles in upper lev number and effective radius of graupel, together led to gre a consequence to stronger electric field intensities. Lightni the electric field intensity is greater than a certain threshold tends to further affect lightning activity through electrifi ation. Mansell et al. (2013) found that greater CCN concentration led to increased lightning activity up to a point, by affecting microphysical and electrical characteristics, with a large sensitivity to ice multiplication. In agreement with Mansell et al. (2013), this study showed that higher CCN concentration in the polluted case result in a relatively strong upper negative charge region, together with increased charge density and electric field intensity, finally enhancing lightning activity, as shown in Fig. 3b.

Hard to understand this sentence structure.

4.4 Convective strength

It is found that vertical conv d significantly under different aerosol conditions (Fig. showed that greater updraft was driven by increased mic ting convection (Wang et al., 2011; Mansell and Ziegler re 10 shows the vertical distribution of latent heat r re stage for both cases. It is evident that the vertical pr km are similar for different conditions. Considerin hat both cases have rather high CCN concentration, there would not be much difference between them in condensation.

Add more recent references.

So, what makes the simulations different?

The peak value of latent heating at higher level (11-14 km) is greater in the polluted case at this stage, with more ice-phase particles appearing (Fig. 7). The maximum latent heating of P-case (greater than 0.025 K s^{-1}), which could be from extra droplet freezing, appears near 12 km, while the latent heating of C-case is only 0.015 K s^{-1} at the same height. Previous studies also found that elevated aerosol loading contributed to the increasing frozen latent heat (e.g., Khain et al., 2005; Lynn et al. 2007; Storer et al., 2010). The increasing release of the latent heat of freezing strengthens the convection and further enhances charging and eventually lightning activity, as discussed above.

https://doi.org/10.5194/acp-2020-1284
Preprint. Discussion started: 18 January 2021

Atmospheric Chemistry and Physics Discussions

However, higher CCN concentration has little influence on condensation at lower level at this stage.

4.5 Delay of first flas

As described abov … discharge was delayed in the polluted situation. In the mea…while, the total charge density of the P-case is also weaker. The vertical charge distribution for the continental and polluted cases at the early development stage are shown in Figure 11d and 12d. It is clear that charge density in the C-case is greater than the P-case. The maximum of positive charge density of the C-case is more than +1 nC m^{-3} at 9 km, while the peak of the P-case is less than +0.5 nC m^{-3}. Compared to the C-case, the area where the charge density > +0.1 nC m^{-3} or < -0.1 nC m^{-3} is much smaller in the P-case (Fig. 12d).

The differences of the charge density are further explored by examining the non-inductive charging mechanism. The polarity and magnitude of non-inductive charging depend on graupel-ice collision, and are related to environmental temperature and LWC, which mainly occurs between -10 ℃ and -40 ℃ with sufficient LWC (Takahashi, 1978; Saunders et al., 1991; Saunders and Peck, 1998; Yair et al., 2010). In the present simulation, positive non-inductive charging rate exceeding 50 pC m^{-3} s^{-1} appears between 8 and 10 km in the C-case (Fig. 11b), corresponding to the positive charge region. Fig. 11a and 11c display the charge carried by different hydrometeors, which indicate graupel charged positively in this region, mainly due to collisions of graupel and ice particles with relatively low temperature (-30 ℃). Compared to the C-case, the non-inductive charging rate is much lower (< 0.5 pC m^{-3} … Fig. 12b), resulting from lower graupel and ice particle concentr… lower collision rates (Fig. 12a and 12c) at the beginning. With … of the thunderstorm and the appearance of more ice-phase par… the charge density > +0.1 nC m^{-3} (or < -0.1 nC m^{-3}) becomes much larger at 09:30 UTC in the P-case (Fig. 13d), when it is more similar to the C-case at 09:18 UTC (Fig. 11d). In the meanwhile, the non-inductive charging rate increases significantly, resulting from the

https://doi.org/10.5194/acp-2020-1284
Preprint. Discussion started: 18 January 2021

appearance of more graupel particles (Fig. 13b).

High CCN concentration forces high concentrations of smaller droplets (Fig. 6a), making coalescence less efficient and delaying precipitation (Mansell and Ziegler, 2013). In the C-case, the earlier appearance of graupel probably led to earlier charging and thus lightning discharges

5 Conclusions and discussion

To elucidate the effects of aerosol on lightning activity, a two-moment bulk microphysics scheme (Mansell et al., 2010; Mansell and Ziegler, 2013) and bulk lightning model (BLM, Fierro et al., 2013) were coupled in the WRF model to simulate a multicell thunderstorm that occurred on 11 August 2017 in the metropolitan Beijing area. The simulated distribution [illegible] development of radar reflectivity are in overall agreement with [illegible]

Sensitivity experiments s[illegible]nd duration of lightning activity are evidently different betw[illegible] moderate (continental) and high (polluted) aerosol concentrations, resulting from microphysical processes. Elevated aerosol loading enhances the development of ice-phase microphysical processes, evidenced by more ice crystals and larger effective radius of graupel participating in charge-separation and electrification processes. As a result, non-inductive charging increases due to more frequent and effective collisions between graupel and other ice-phase particles. These lead to higher charge density, together with larger upper negative charge region which is caused [illegible] particles transported to higher levels, leading to electric fields t[illegible] breakdown value, culminating in an enhanced lightning activity [illegible] and mature stages of the thunderstorm, the latent heat release [illegible] noticeably greater in the P-case, mainly due to the release of latent heat during freezing of supercooled liquid particles. But higher CCN concentration has little influence on condensation at lower level at later stage compared to the continental CCN concentration, which already limits the development of excess supersaturation.

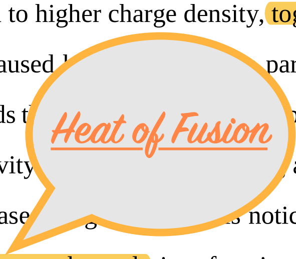

https://doi.org/10.5194/acp-2020-1284
Preprint. Discussion started: 18 January 2021

Compared to the C-case, initial lightning activity was delayed at the beginning of polluted thunderstorm in the P-case. A delay of the first flash was also found by Tan et al. (2017), however, the advanced growth of graupel and ice crystals at the initiative time with lower CCN was not noted. In this study, raindrops and graupel appear earlier under continental condition at the beginning due to relatively efficient coalescence, helping to make downdrafts and lead to earlier non-ind[illegible] and lightning.

Observation and simulation studies found [illegible] nhanced the electrical activity (e.g., Koren et al., 2[illegible] vious studies suggested that the mass mixing rat[illegible] th the enhanced CCN concentration, eventually resu[illegible] vity (e.g., Wang et al., 2011; Zhao et al., 2015), whi[illegible] decrease of graupel mixing ratio was found by Tan et al. (2017). It should be noted that when aerosol concentrations are too large, this leads to the inhibition of convection resulting in less lightning, as discovered by Altaratz et al. (2010) in the Amazon basin, as well as by Hu et al. (2019) in Houston region, and simulated by Mansell and Ziegler (2013). In this study, the enhancement of lightning activity under polluted condition results from increasing ice crystal number and effective radius of graupel particles. More ice-phase particles in upper level under polluted condition, forming a relatively stronger negative charge region above the main positive charge center, which is also indicated by Zhao et al. (2015). We found that under continental condition, earlier charging results from advanced occurrence of graupel and ice crystals, providing support for the result of first discharge delay in the polluted thunderclouds (Tan et al., 2017).

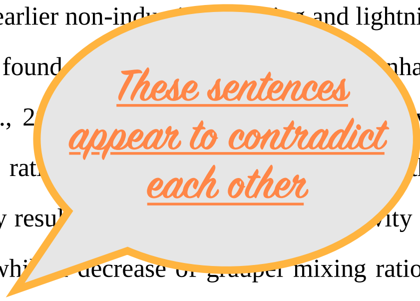

The impacts of aerosol on lightning were investigated acting as CCN, however, aerosol also tends to affect electrification and lightning discharge by acting as ice nuclei (IN) through microphysical processes (Tao et al., 2012; Fan et al., 2017). More sensitive experiments are still needed to discuss the influences of aerosol on lightning due to microphysical and thermodynamic processes, acting as IN.

Data availability

To request the data given in this study, please contact Dr. Dongxia Liu at the Institute of Atmospheric Physics, Chinese Academy of Sciences, via email (liudx@mail.iap.ac.cn).

Author contributions

MS, XQ designed the research ideas for this study. MS carried the study out and prepared the paper. EM provided analysis ideas for the microphysics and electrification. DL and YY edited the paper. Other co-authors participated in science discussions and article modification.

Competing interests

The authors declare that they have no conflict of interest.

Acknowledgment

This research was supported by an NSFC-ISF grant (Nos. 41761144074, 2640/17), and the National Natural Science Foundation of China (Nos. 41630425, 41875007).

Reference

Altaratz O, Kucienska B, Kostinski A B, et al. Global association of aerosol with flash density of intense lightning[J]. Environmental Research Letters, 2017, 12(11).

Altaratz O, Koren I, Yair Y, et al. Lightning response to smoke from Amazonian fires[J]. Geophysical Research Letters, 2010, 37(7).

Brooks I M, Saunders C P R, Mitzeva R P, et al. The effect on thunderstorm charging of the rate of rime accretion by graupel[J]. Atmospheric Research, 1997, 43(3): 277-295.

https://doi.org/10.5194/acp-2020-1284
Preprint. Discussion started: 18 January 2021

Chaudhuri S, Middey A. Effect of meteorological parameters and environmental pollution on thunderstorm and lightning activity over an urban metropolis of India[J]. Urban Climate, 2013, 3: 67-75.

Dye J E, Knight C A, Toutenhoofd V, et al. The Mechanism of Precipitation Formation in Northeastern Colorado Cumulus III. Coordinated Microphysical and Radar Observations and Summary[J]. Journal of the Atmospheric Sciences, 1974, 31(8): 2152-2159.

Fan J, Zhang R, Li G, et al. Effects of aerosols and relative humidity on cumulus clouds[J]. Journal of Geophysical Research: Atmospheres, 2007, 112(D14).

Fan J, Leung L R, Rosenfeld D, et al. Effects of cloud condensation nuclei and ice nucleating particles on precipitation processes and supercooled liquid in mixed-phase orographic clouds[J]. Atmospheric Chemistry and Physics, 2017, 17(2).

Fierro A O, Mansell E R, Mac Gorman D R, et al. The implementation of an explicit charging and discharge lightning scheme within the WRF-ARW model: Benchmark simulations of a continental squall line, a tropical cyclone, and a winter storm[J]. Monthly Weather Review, 2013, 141(7): 2390-2415.

Guo J, Deng M, Lee S S, et al. Delaying precipitation and lightning by air pollution over the Pearl River Delta. Part I: Observational analyses[J]. Journal of Geophysical Research: Atmospheres, 2016, 121(11): 6472-6488.

Hobbs P V, Rangno A L. Ice Particle Concentrations in Clouds[J]. Journal of the Atmospheric Sciences, 1985, 42(23): 2523-2549.

Hu J, Rosenfeld D, Ryzhkov A, et al. Polarimetric radar convective cell tracking reveals large sensitivity of cloud precipitation and electrification properties to CCN[J]. Journal of Geophysical Research: Atmospheres, 2019, 124(22): 12194-12205.

Jayaratne E R, Saunders C P R, Hallett J. Laboratory studies of the charging of soft-hail during ice crystal interactions[J]. Quarterly Journal of the Royal Meteorological Society, 1983, 109(461): 609-630.

Jiang M, Feng J, Sun R, et al. Potential influences of neglecting aerosol effects on the NCEP GFS precipitation forecast[J]. Atmospheric Chemistry and Physics, 2017, 17(22):13967-13982.

https://doi.org/10.5194/acp-2020-1284
Preprint. Discussion started: 18 January 2021

Atmospheric Chemistry and Physics Discussions
Open Access
EGU

Kar S K, Liou Y A, Ha K J. Aerosol effects on the enhancement of cloud-to-ground lightning over major urban areas of South Korea[J]. Atmospheric Research, 2009, 92(1):0-87.

Khain A, Rosenfeld D, Pokrovsky A. Aerosol impact on the dynamics and microphysics of deep convective clouds[J]. Quarterly Journal of the Royal Meteorological Society: A journal of the atmospheric sciences, applied meteorology and physical oceanography, 2005, 131(611): 2639-2663.

Khain A, Cohen N, Lynn B, et al. Possible Aerosol Effects on Lightning Activity and Structure of Hurricanes[J]. Journal of the Atmospheric Sciences, 2008, 65(12):3652-3677.

Lynn B, Khain A, Rosenfeld D, et al. Effects of aerosols on precipitation from orographic clouds[J]. Journal of Geophysical Research: Atmospheres, 2007, 112(D10).

MacGorman D R, Rust W D, Schuur T J, et al. TELEX the thunderstorm electrification and lightning experiment[J]. Bulletin of the American Meteorological Society, 2008, 89(7): 997-1014.

Mansell E R, Ziegler C L. Aerosol effects on simulated storm electrification and precipitation in a two-moment bulk microphysics model[J]. Journal of the Atmospheric Sciences, 2013, 70(7): 2032-2050.

Mansell E R, Ziegler C L, Bruning E C. Simulated electrification of a small thunderstorm with two-moment bulk microphysics[J]. Journal of the Atmospheric Sciences, 2010, 67(1): 171-194.

Mansell E R, MacGorman D R, Ziegler C L, et al. Charge structure and lightning sensitivity in a simulated multicell thunderstorm[J]. Journal of Geophysical Research: Atmospheres, 2005, 110(D12).

Mitzeva R, Latham J, Petrova S. A comparative modeling study of the early electrical development of maritime and continental thunderstorms[J]. Atmospheric research, 2006, 82(1-2): 26-36.

Naccarato K P, Pinto Jr O, Pinto I. Evidence of thermal and aerosol effects on the cloud-to-ground lightning density and polarity over large urban areas of Southeastern

Brazil[J]. Geophysical Research Letters, 2003, 30(13).

Orville R E, Huffines G, Nielsen‐Gammon J, et al. Enhancement of cloud-to-ground lightning over Houston, Texas[J]. Geophysical Research Letters, 2001, 28(13): 2597-2600.

Price C. Global surface temperatures and the atmospheric electrical circuit[J]. Geophysical Research Letters, 1993, 20(13): 1363-1366.

Price C, Rind D. A simple lightning parameterization for calculating global lightning distributions[J]. Journal of Geophysical Research Atmospheres, 1992, 97(D9):9919-9933.

Qie X, Yuan S, Chen Z, et al. Understanding the dynamical-microphysical-electrical processes associated with severe thunderstorms over the Beijing metropolitan region[J]. Science China Earth Sciences, 2020: 1-17.

Qie X, Yuan T, Xie Y, et al. Spatial and temporal distribution of lightning activities on the Tibetan Plateau[J]. Chinese Journal of Geophysics, 2004, 47(6): 1122-1127.

Reynolds S E, Brook M, Gourley M F. Thunderstorm charge separation[J]. Journal of Meteorology, 1957, 14(5): 426-436.

Rosenfeld D, Lohmann U, Raga G B, et al. 2008. Flood or drought: How do aerosols affect precipitation?[J]. Science, 321(5894): 1309-1313.

Rosenfeld D, Woodley W L. 2000. Deep convective clouds with sustained supercooled liquid water down to -37.5 ℃[J]. Nature, 405(6785): 440.

Saunders C P R, Peck S L. Laboratory studies of the influence of the rime accretion rate on charge transfer during crystal/graupel collisions[J]. Journal of Geophysical Research: Atmospheres, 1998, 103(D12): 13949-13956.

Saunders C P R, Keith W D, Mitzeva R P. The effect of liquid water on thunderstorm charging[J]. Journal of Geophysical Research: Atmospheres, 1991, 96(D6): 11007-11017.

Srivastava A, Tian Y, Qie X S, et al. 2017. Performance assessment of Beijing Lightning Network (BLNET) and comparison with other lightning location networks across Beijing. Atmospheric Research, 197 76-83.

Stolz D C, Rutledge S A, Pierce J R. Simultaneous influences of thermodynamics and aerosols on deep convection and lightning in the tropics[J]. Journal of Geophysical Research: Atmospheres, 2015, 120(12): 6207-6231.

Storer R L, Van Den Heever S C, Stephens G L. Modeling aerosol impacts on convective storms in different environments[J]. Journal of the Atmospheric Sciences, 2010, 67(12): 3904-3915.

Sun M, Qie X, Liu D, et al. Analysis of potential effects of aerosol on lightning activity in Beijing metropolitan region[J]. Chinese Journal of Geophysics, 2020, 63(5): 1766-1774.

Takahashi T. A numerical simulation of winter cumulus electrification. Part I: Shallow cloud[J]. Journal of the Atmospheric Sciences, 1983, 40(5): 1257-1280.

Takahashi T. Riming electrification as a charge generation mechanism in thunderstorms[J]. Journal of the Atmospheric Sciences, 1978, 35(8): 1536-1548.

Tan Y B, Ma X, Xiang C Y, et al. A numerical study of the effects of aerosol on electrification and lightning discharges during thunderstorms[J]. Chinese Journal of Geophysics, 2017, 60(8): 3041-3050.

Tao W K, Chen J P, Li Z, et al. Impact of aerosols on convective clouds and precipitation[J]. Reviews of Geophysics, 2012, 50(2).

Thomas R J, Krehbiel P R, Rison W, et al. Observations of VHF source powers radiated by lightning[J]. Geophysical Research Letters, 2001, 28(1): 143-146.

Thornton J A, Virts K S, Holzworth R H, et al. 2017. Lightning enhancement over major oceanic shipping lanes[J]. Geophysical Research Letters, 44(17).

Twomey, S., 1959: The nuclei of natural cloud formation, Part II: The supersaturation in natural clouds and the variation of cloud droplet concentration. Geofis. Pura Appl., 43, 243–249.

Wang Q, Li Z, Guo J, et al. 2018. The climate impact of aerosols on the lightning flash rate: is it detectable from long-term measurements?[J]. Atmospheric Chemistry and Physics, 18(17).

Wang Y, Qie X S, Wang D F, et al. 2016. Beijing Lightning Network (BLNET) and the observation on preliminary breakdown processes [J]. Atmos. Res., 171: 121–132.

Wang Y, Wan Q, Meng W, et al. Long-term impacts of aerosols on precipitation and lightning over the Pearl River Delta megacity area in China[J]. Atmospheric Chemistry and Physics, 2011, 11(23): 12421-12436.

Westcott N E. Summertime cloud-to-ground lightning activity around major Midwestern urban areas[J]. Journal of Applied Meteorology, 1995, 34(7): 1633-1642.

Williams E, Mushtak V, Rosenfeld D, et al. Thermodynamic conditions favorable to superlative thunderstorm updraft, mixed phase microphysics and lightning flash rate[J]. Atmospheric Research, 2005, 76(1-4): 288-306.

Williams E, Stanfill S. The physical origin of the land–ocean contrast in lightning activity[J]. Comptes Rendus Physique, 2002, 3(10): 1277-1292.

Williams E. The tripole structure of thunderstorms[J]. Journal of Geophysical Research, 1989: 13151-13167.

Xiong Y J, Qie X S, Zhou Y J, et al. Regional responses of lightning activities to relative humidity of the surface[J]. Chinese Journal of Geophysics, 2006, 49(2): 311-318.

Yair Y. Lightning hazards to human societies in a changing climate[J]. Environmental Research Letters, 2018, 13(12).

Yair Y, Lynn B, Price C, et al. Predicting the potential for lightning activity in Mediterranean storms based on the Weather Research and Forecasting (WRF) model dynamic and microphysical fields[J]. Journal of Geophysical Research, 2010.

Yair Y. Charge generation and separation processes[J]. Space Science Reviews, 2008, 137(1-4): 119-131.

Yuan T, Remer L A, Pickering K E, et al. Observational evidence of aerosol enhancement of lightning activity and convective invigoration[J]. Geophysical Research Letters, 2011, 38(4).

Zhao P, Li Z, Xiao H, et al. Distinct aerosol effects on cloud-to-ground lightning in the plateau and basin regions of Sichuan, Southwest China[J]. Atmospheric Chemistry and Physics, 2020, 20(21): 13379-13397.

Zhao P, Yin Y, Xiao H. The effects of aerosol on development of thunderstorm electrification: A numerical study[J]. Atmospheric Research, 2015, 153: 376-391.

https://doi.org/10.5194/acp-2020-1284
Preprint. Discussion started: 18 January 2021

Ziegler C L. Retrieval of thermal and microphysical variables in observed convective storms. Part 1: Model development and preliminary testing[J]. Journal of the Atmospheric Sciences, 1985, 42(14): 1487-1509.

https://doi.org/10.5194/acp-2020-1284
Preprint. Discussion started: 18 January 2021

Atmospheric Chemistry and Physics
Discussions

Table1. Settings for the nested simulations

Model Option	**Outer D01**	**Inner D02**
Domain Coverage	6km, 442×391	2km, 496×496
Vertical levels	40	40
Time step	30s	10s
Microphysics Scheme	NSSL	NSSL
Longwave Radiation	RRTM	RRTM
Shortwave Radiation	Dudhia	Dudhia
Boundary Layer	BouLac PBL	BouLac PBL
Land Surface	Unified Noah LSM	Unified Noah LSM

https://doi.org/10.5194/acp-2020-1284
Preprint. Discussion started: 18 January 2021

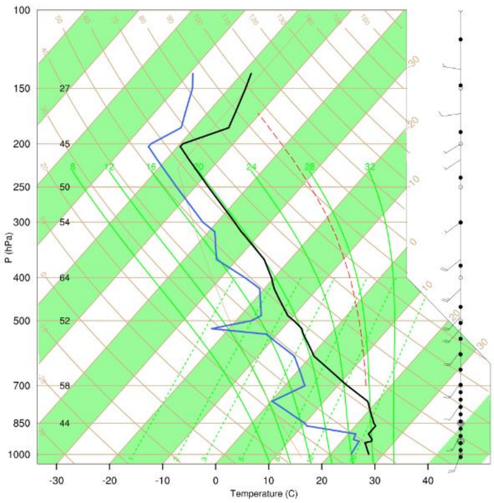

Figure 1 Sounding profiles for Beijing at 12:00 UTC on Aug11, 2017. The black, blue solid lines and red dashed line represent temperature, dew point, parcel adiabatic lapse rate, respectively.

640

https://doi.org/10.5194/acp-2020-1284
Preprint. Discussion started: 18 January 2021

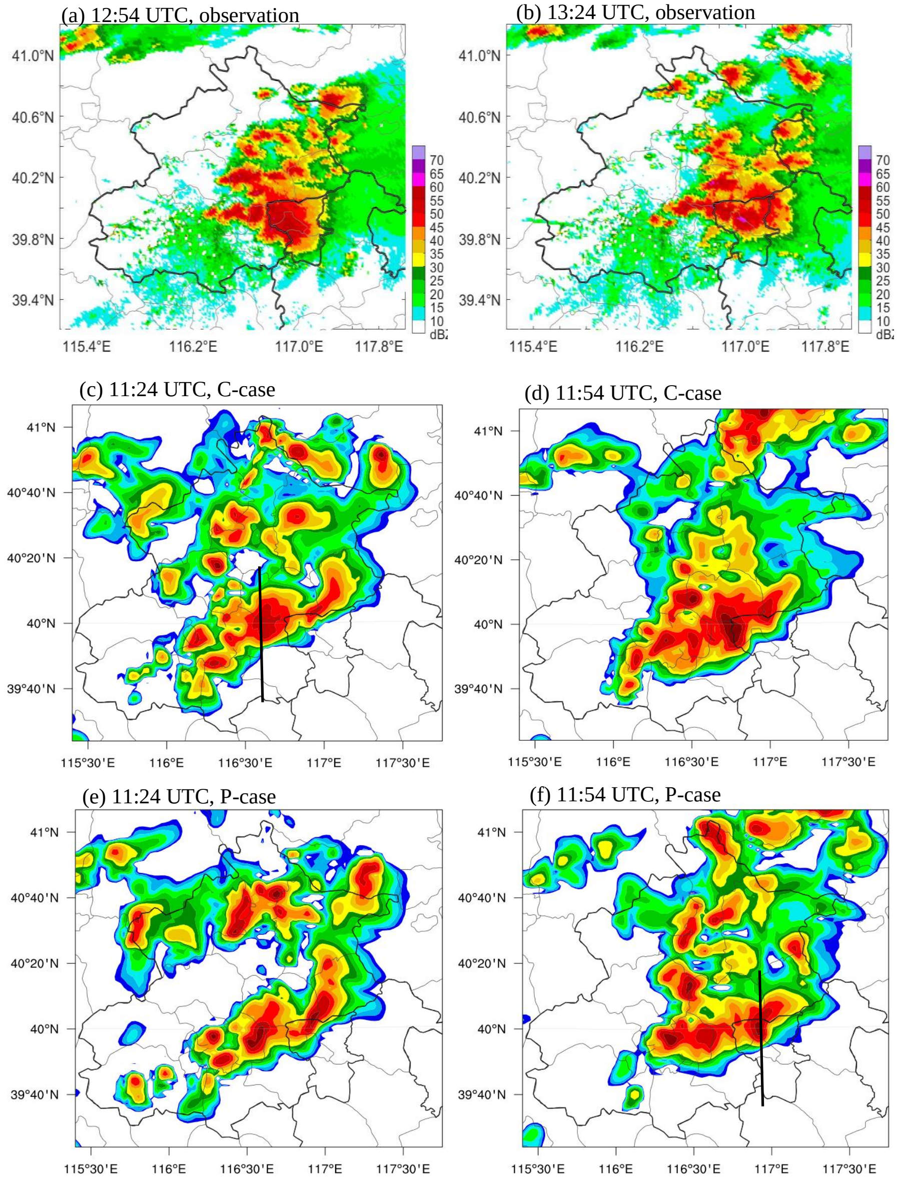

645 **Figure 2** Radar reflectivity (unit: dBZ) between observation and simulation for the C- and P-cases, the simulation was earlier than observation about 1.5 h. (a)-(b) Observation at 12:54 UTC and 13:24 UTC. (c)-(d) Simulation for the C-case at 11:24 UTC and 11:54 UTC. (e)-(f) Simulation for the P-case at 11:24 UTC and 11:54 UTC, respectively.

https://doi.org/10.5194/acp-2020-1284
Preprint. Discussion started: 18 January 2021

Atmospheric Chemistry and Physics
Open Access
EGU
Discussions

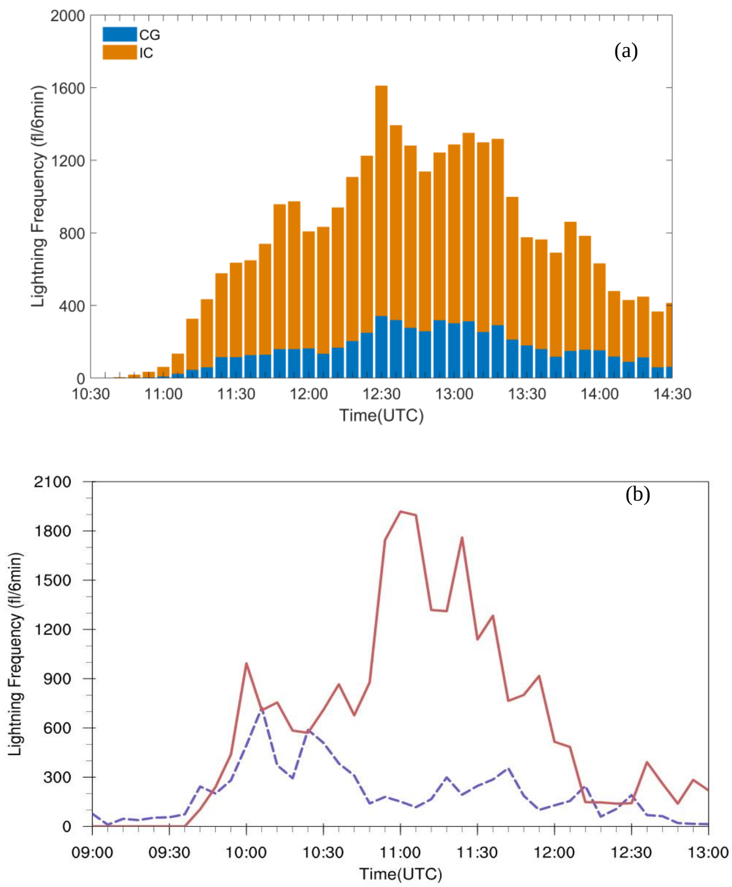

Figure 3 Temporal variation in (a) observed total lightning frequency and (b) simulated lightning frequency. In (a), orange represents IC lightning and blue represents CG lightning. In (b), solid line represents the P-case and dashed line represents the C-case.

https://doi.org/10.5194/acp-2020-1284
Preprint. Discussion started: 18 January 2021

Atmospheric Chemistry and Physics
Discussions

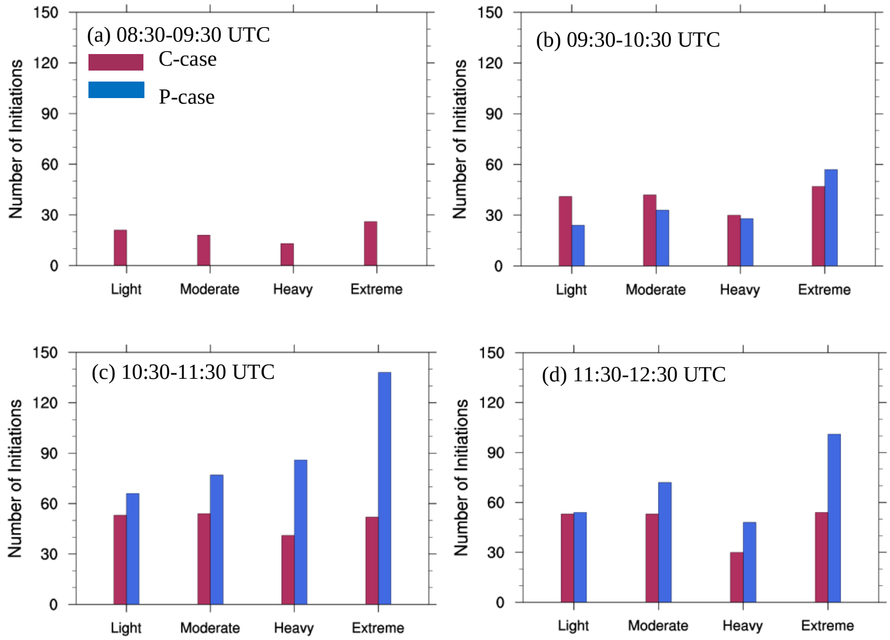

660 **Figure 4** Number of initiations for different lightning categories in different time, i.e. light (50-100 grids), moderate (100-200 grids), heavy (200-300 grids) and extreme (>300 grids), simulated for the P- and C-cases.

https://doi.org/10.5194/acp-2020-1284
Preprint. Discussion started: 18 January 2021

Atmospheric Chemistry and Physics
Open Access
Discussions
EGU

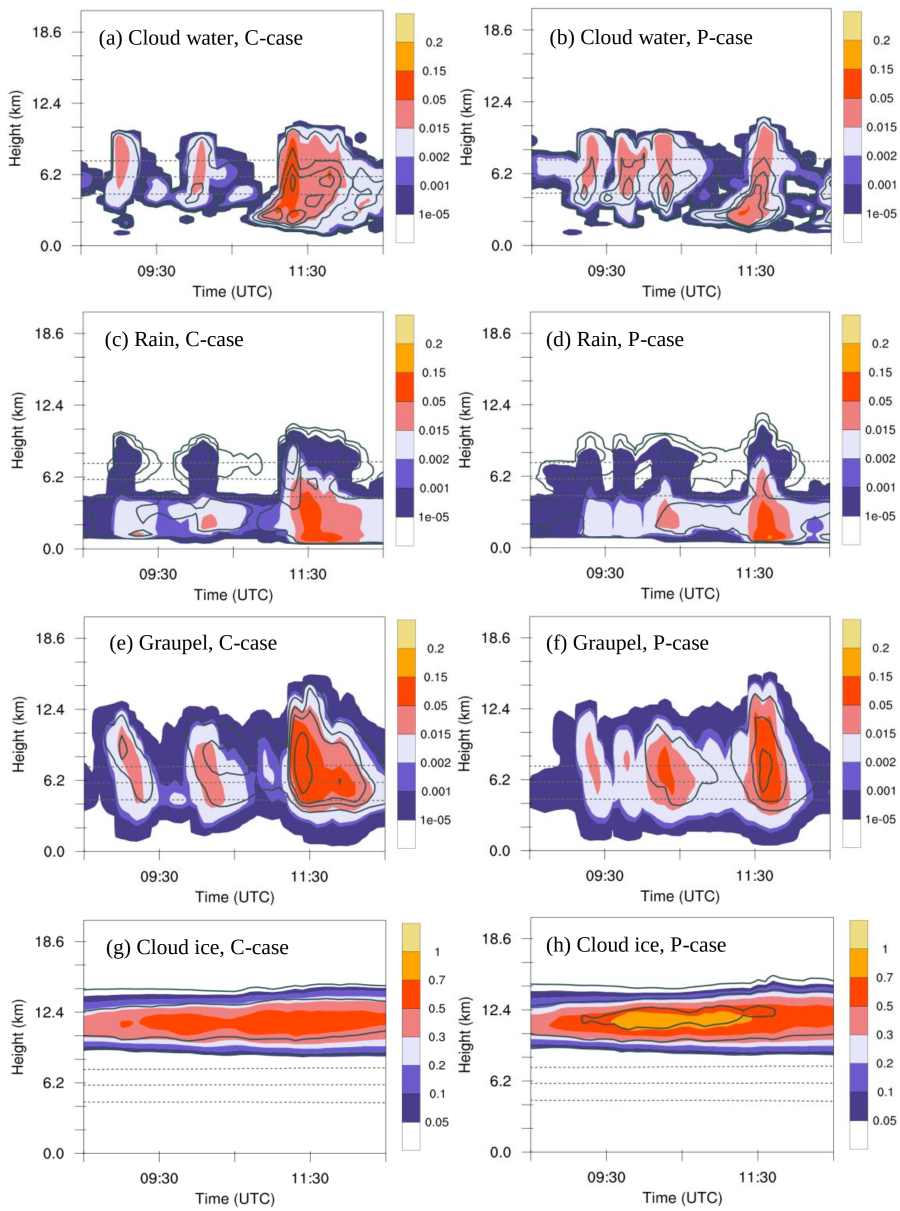

(figure continued on next page)

https://doi.org/10.5194/acp-2020-1284
Preprint. Discussion started: 18 January 2021

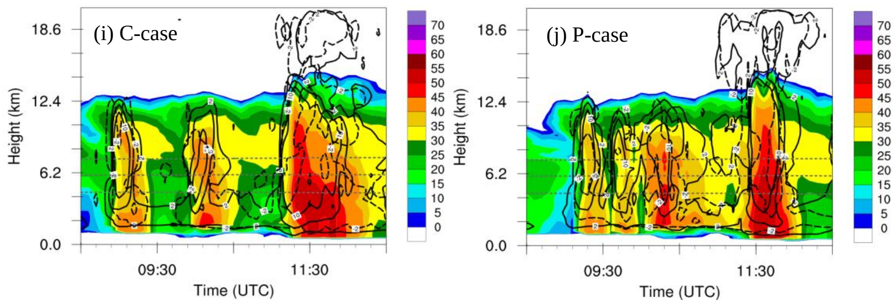

Figure 5 (a)-(h) Temporal variation of the vertical profiles of domain-averaged mass mixing ratio (g kg^{-1}, shaded) and number concentration (kg^{-1}, solid lines) of (a) cloud water in the C-case, (b) cloud water in P-case, (c) rain water in the C-case, (d) rain water in the P-case, (e) graupel in the C-case, (f) graupel in the P-case, (g) ice in the C-case, and (h) ice in the P-case. The 0 ℃, -10 ℃, and -20 ℃ isotherms are shown by the dashed gray lines in (a)-(h). Contour levels in (a)-(h) for cloud water number concentration are 10^5, 10^6, 10^7, 2×10^7, 3×10^7 kg^{-1}, and for rain water are 1, 10, 10^2, 10^3, 3×10^3 kg^{-1}, and for graupel are 10, 30, 50, 100, 300, 500, 700, 1000 kg^{-1}, and for ice are 0.1×10^7, 1×10^7, 3×10^7 kg^{-1}. (i)-(j) Time-height maximum simulated radar reflectivity (color shading, unit: dBZ) and vertical velocities (solid line: 2, 10 m s^{-1}; dashed line: -2 m s^{-1}) for (i) the C-case and (j) the P-case.

https://doi.org/10.5194/acp-2020-1284
Preprint. Discussion started: 18 January 2021

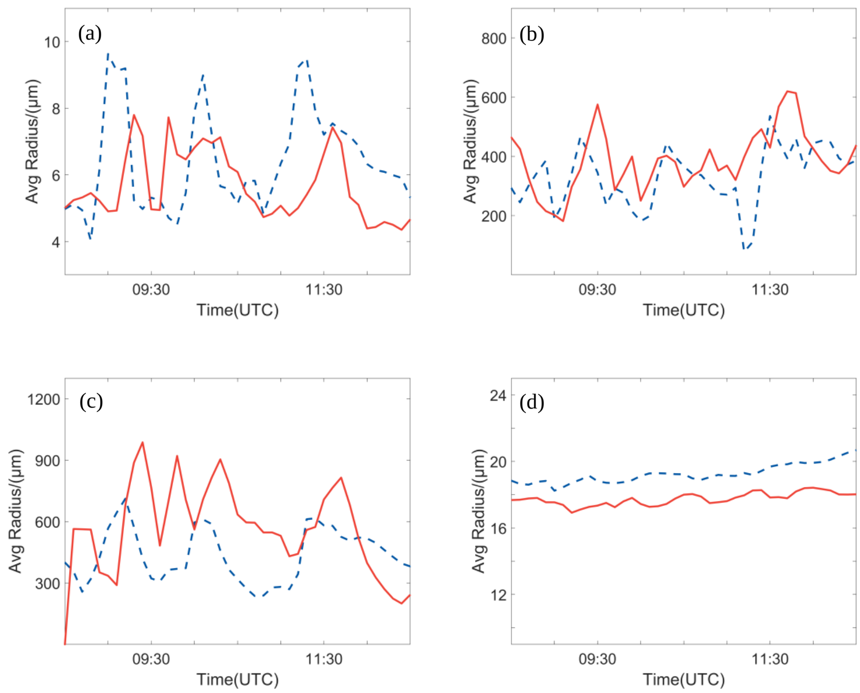

685 **Figure 6** Temporal variation of domain-averaged effective radius for the different hydrometeors. (a) cloud water, (b) rainwater, (c) graupel, (d) ice. The solid lines represent the P-case and the dashed lines represent the C-case.

https://doi.org/10.5194/acp-2020-1284
Preprint. Discussion started: 18 January 2021

Atmospheric Chemistry and Physics
Open Access
Discussions

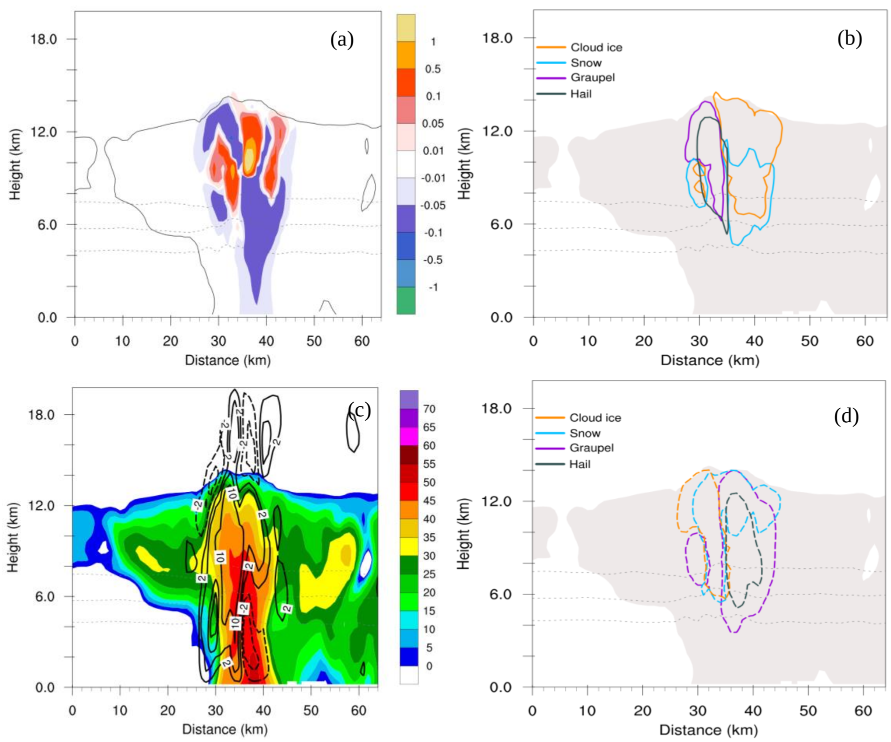

Figure 7 Vertical cross sections (south to north) at the location shown in Fig. 2f of the main electrical and microphysical variables at the mature stage of the thunderstorm (11:54 UTC) in the P-case. (a) Total net space charge (nC m^{-3}, shaded). The 0 ℃, -10 ℃, and -20 ℃ isotherms are shown by dashed gray lines in (a)-(d). (b) +0.1 nC m^{-3} space charge density contours for cloud ice (orange), snow (blue), graupel (purple), and hail (black). The cloud outline (reflectivity echoes ≥5 dBZ) is denoted by the gray shaded contour. (c) Radar reflectivity (unit: dBZ), black lines for vertical velocities (solid line: 2, 5, 10 m s^{-1}; dashed line: -2 m s^{-1}). (d) As in (b), but for -0.1 nC m^{-3} charge density.

https://doi.org/10.5194/acp-2020-1284
Preprint. Discussion started: 18 January 2021

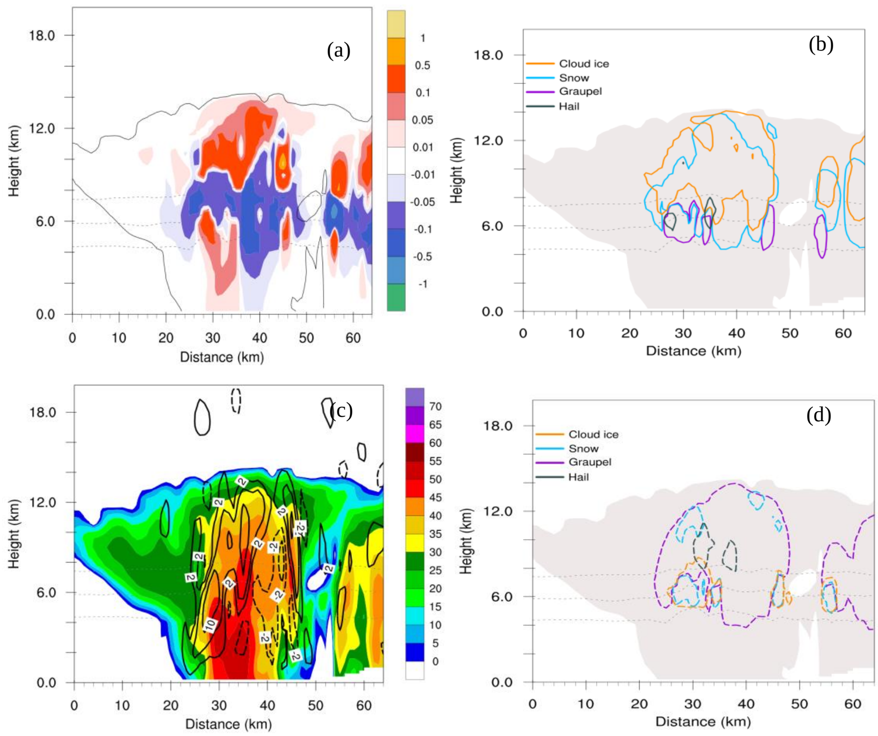

Figure 8 As in Fig. 7, but the vertical cross sections at the location shown in Fig. 2c of the main electrical and microphysical variables at the mature stage of the thunderstorm (11:24 UTC) in the C-case.

https://doi.org/10.5194/acp-2020-1284
Preprint. Discussion started: 18 January 2021

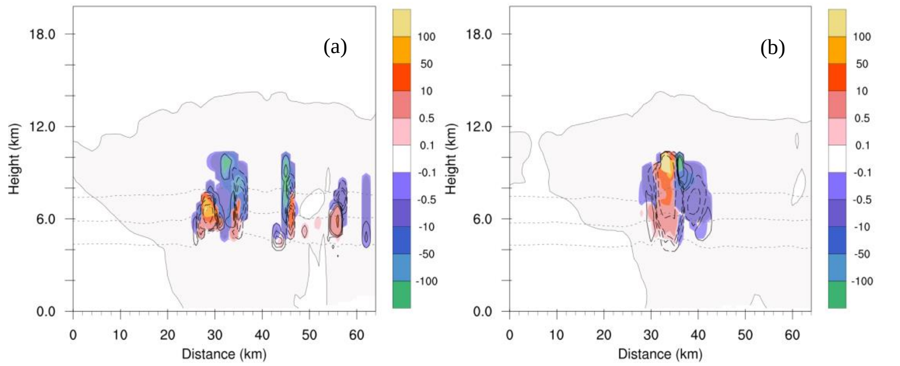

Figure 9 Vertical cross sections (south to north) at the location shown in Fig. 2 of non-inductive (pC m^{-3} s^{-1}, shaded) and inductive (solid lines: 0.1, 0.5, 1 pC m^{-3} s^{-1}; dashed lines: -0.1, -0.5, -1, -5, -10 pC m^{-3} s^{-1}) charging rates at the mature stage of (a) C-case (11:24 UTC, Fig. 2c), and (b) P-case (11:54 UTC, Fig. 2f). The 0 °C, -10 °C, and -20 °C isotherms are shown by dashed gray lines.

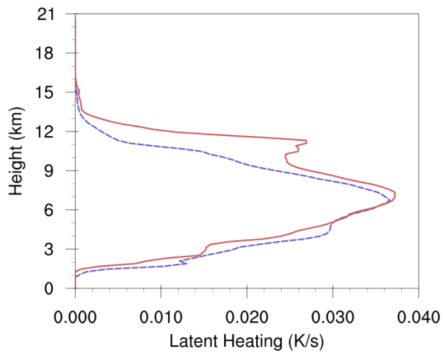

Figure 10 Vertical profiles of domain-maximum latent heating (unit: K s^{-1}), at the developing and mature stage (09:30-12:00 UTC). The solid line represents the P-case and the dashed line represents the C-case.

https://doi.org/10.5194/acp-2020-1284
Preprint. Discussion started: 18 January 2021

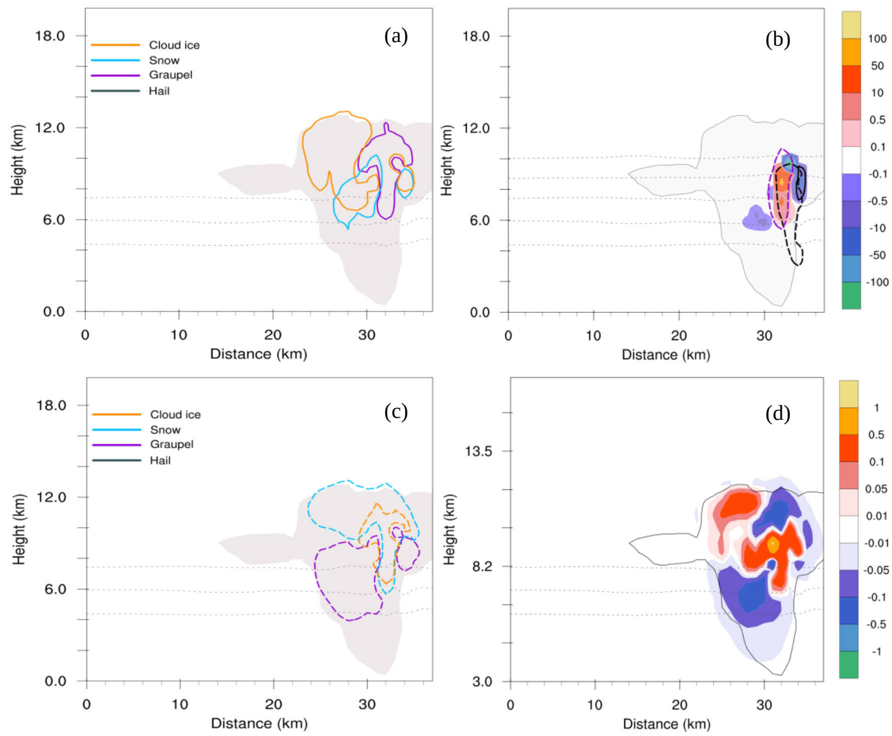

Figure 11 Vertical cross sections (south to north) of main electrical and microphysical variables at the beginning of the thunderstorm (09:18 UTC) in the C-case. (a) +0.1 nC m^{-3} space charge density contours for cloud ice (orange), snow (blue), graupel (purple), and hail (black). The cloud outline (reflectivity echoes ≥5 dBZ) is denoted by the gray shaded contour. (b) Non-inductive (shaded) and inductive (solid black line) charging rate (unit: pC m^{-3} s^{-1}), dashed black line for LWC (1 g kg^{-1}), dashed violet line for graupel (0.5, 3 g kg^{-1}). (c) As in (a), but for -0.1 nC m^{-3} charge density. (d) Total net space charge (nC m^{-3}, shaded). The 0 °C, -10 °C, and -20 °C isotherms are shown by dashed gray lines in (a)-(d).

https://doi.org/10.5194/acp-2020-1284
Preprint. Discussion started: 18 January 2021

Atmospheric Chemistry and Physics Discussions

735

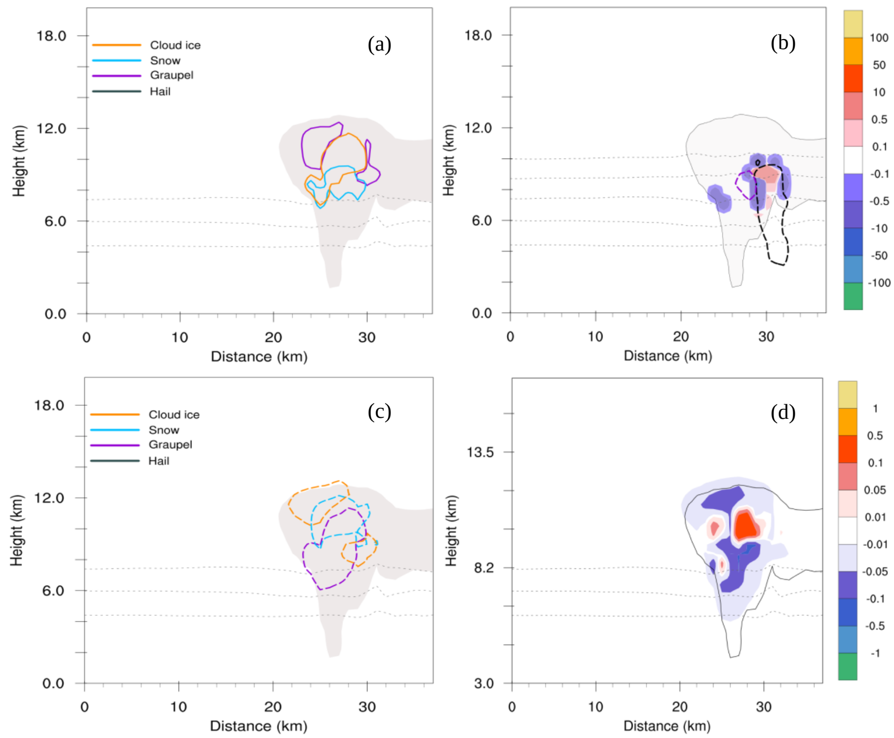

Figure 12 As in Fig. 11, but the vertical cross sections at the beginning of the thunderstorm (09:18 UTC) in the P-case.

https://doi.org/10.5194/acp-2020-1284
Preprint. Discussion started: 18 January 2021

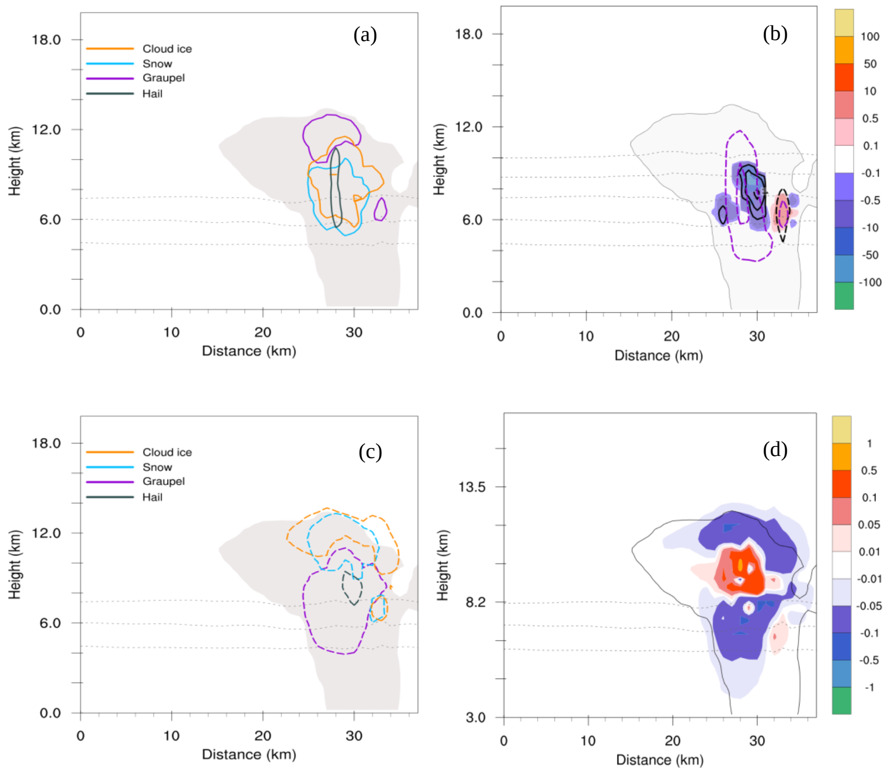

Figure 13 As in Fig. 11, but the vertical cross sections later than the beginning of the thunderstorm (09:30 UTC) in the P-case.